Journal of Ceramic Processing Research. Vol. 22, No. 5, pp. 576~583 (2021)
(Received 18 April 2021, Received in revised form 4 July 2021, Accepted 17 July 2021)
https://doi.org/10.36410/jcpr.2021.22.5.576

J O U R N A L O F
Ceramic Processing Research

Preparation and oxygen desorption performance modification of $BaCoO_{3-\delta}$ perovskite-type materials via B-site cerium doping

Qiuwan Shen[a], Zicheng Shao[a], Yuhang Jiang[a], Shian Li[a,*], Guogang Yang[a], Naibao Huang[b], and Xinxiang Pan[a]
[a]*Marine Engineering College, Dalian Maritime University, Dalian, China*
[b]*College of Transportation Engineering, Dalian Maritime University, Dalian, China*

The oxyfuel combustion process is used as a potential technique to CO_2 capture and the oxygen carries play a crucial role of this technology. Ba-Co based perovskites are promising materials to producing O_2/CO_2 gas for oxyfuel combustion. In this study, perovskite oxides $BaCo_{0.8}M_{0.2}O_{3-\delta}$ (M = Ce, Al, Fe, Cu) were prepared via an EDTA sol-gel method. Scanning electron microscope (SEM) was used to study the surface morphology and structure of the fresh and the used perovskite powders. Oxygen adsorption/desorption experiments were carried out in a fixed-bed system; and the oxygen desorption property of $BaCo_{0.8}Ce_{0.2}O_{3-\delta}$ was studied in details. The oxygen production amount of 1g $BaCo_{0.8}Ce_{0.2}O_{3-\delta}$ perovskite powders can reach 101.07 mg after one adsorption and desorption cycle. SEM results showed that the fresh samples had a porous structure; however the particles were covered by impurities after cycles due to the sintering. Experiments results indicated that the optimal desorption temperature is 850°C. The optimal volume flow rate of carbon dioxide and partial pressures of carbon dioxide were determined to be 200 $ml \cdot min^{-1}$, 100% CO_2 partial pressure, respectively. Furthermore, the results of cyclic performance indicate that $BaCo_{0.8}Ce_{0.2}O_{3-\delta}$ perovskite powder shows high cyclic stability for producing O_2-enriched CO_2 stream.

Keywords: Oxyfuel combustion, CO_2 capture, oxygen desorption, doping

Introduction

The CO_2 emission from fossil fuels combustion has been the focus of attention all over the world in recent years [1]. The Intergovernmental Panel on Climate Change (IPCC) offers a potential options-carbon capture and storage (CCS) to reduce CO_2 emissions [2]. The oxyfuel technique is supposed to possess a potential CCS for extensive promotion and commercial potential [3-5]. Oxyfuel combustion is a versatile technology that can be combined with electricity, synthetic fuel, and in energy-intensive industries such as cement and steel. Fig. 1 displays a diagrammatic sketch of an oxyfuel combustion system [6-8]. However, Barriers for traditional oxyfuel combustion is the high investment of pure oxygen gas which is produced by cryogenic method [9].

Perovskite oxides can supply O_2/CO_2 flow at high temperature which could be applied for oxyfuel combustion application [10]. Fig. 2 shows the system of producing oxygen-enriched CO_2 stream: (1) In the adsorption process, air is adopted as an inlet gas to saturate the perovskite with O_2; (2) In the desorption process, oxygen is desorbed when carbon dioxide is applied as a purge gas, as well as producing an O_2/CO_2 mixed gas. This cyclic process of oxygen adsorption and desorption is reversible. According to the research results of Shen [11] et al, it can be inferred that this process can be expressed as:

$$BaCo_{0.8}B_{0.2}O_{3-\delta} + CO_2 \leftrightarrow BaCO_3 + 0.8CoO + 0.1B_2O_3 + \frac{0.9-\delta}{2}O_2 \quad (1)$$

Perovskite oxides with general formula ABO_3 possess unique properties, such as oxidizing, ferroelectricity and superconductivity, which make them attractive in various technological applications [12-17]. The idealized crystal structure of ABO_3 is drawn in Fig. 3. The structural formula of perovskite oxides is ABO_3, where A-cations are located on the edge of the crystal structure and play a major role in stabilization, and B-cations are located in the center of structure [18].

To be a promising sorbent material, perovskites must have high oxygen adsorption capacity and high adsorption/desorption capacity. Perovskite-type metal oxides usually require a higher reaction temperature. Therefore, many researchers studied the oxygen absorption/desorption capacity by A/B-site doping on perovskites [19, 20]. Li et al. found the B-site substitution has a significant effect on the O_2 desorption performance and reactivity of cobalt-based perovskites [21]. Additionally, they found that the O_2 desorption amount of B-site substitution was in the order: $LaNiO_{3-\delta}$ > $LaCoO_{3-\delta}$ >

*Corresponding author:
Tel : +86-13190160896
Fax: +0411-84728659
E-mail: lishian@dlmu.edu.cn

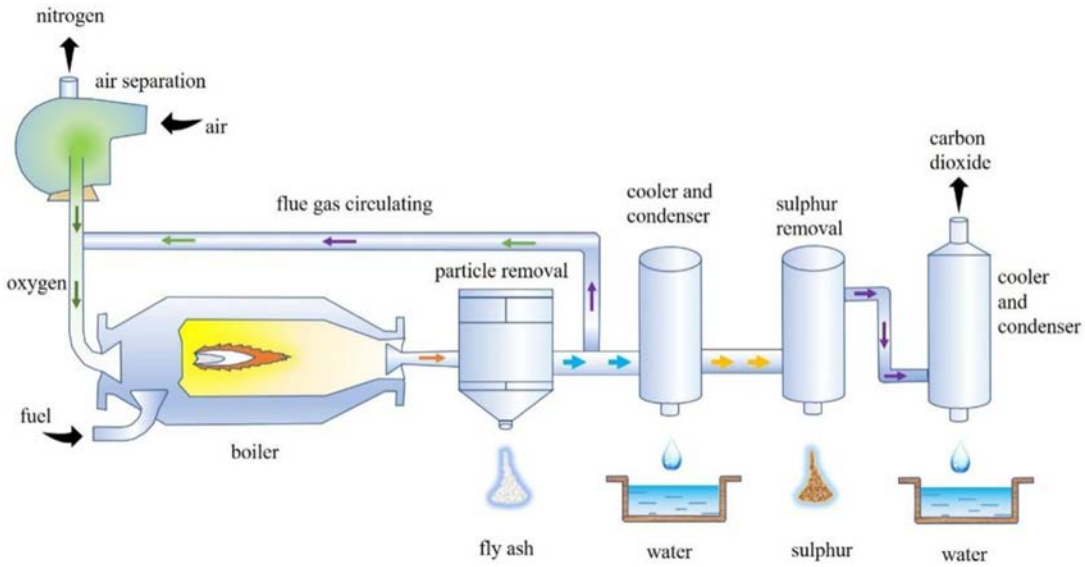

Fig. 1. Diagrammatic sketch of an oxyfuel combustion system.

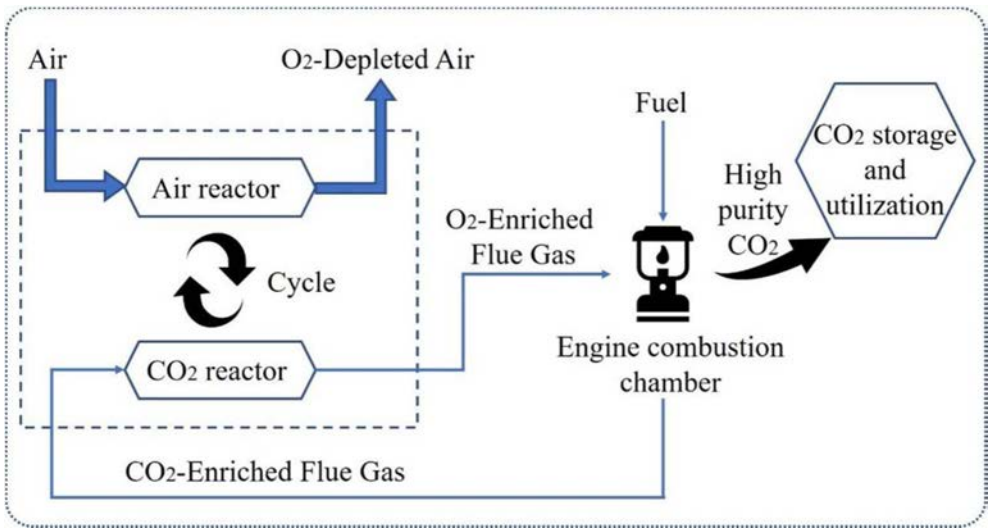

Fig. 2. Schematic diagram of producing oxygen-enriched CO_2 stream.

$LaCrO_{3-\delta}$ > $LaFeO_{3-\delta}$ and the perovskite supported by CeO_2 showed the best oxygen desorption performance. This is due to the fact that active oxygen species in cerium oxide can be supplied to perovskite at high temperatures [22]. In addition, Shen et al. indicated that the cobalt-based perovskites, with high oxygen permeation flux, is a potential oxygen carrier material [23]. Ding et al. synthesized a series of A/B site substitution $Ba_{1-x}Sr_xCo_{1-y}Fe_yO_{3-\delta}$ by sol-gel method [24]. They found that the optimal pressure was 2 MPa and the optimal temperature was 850 °C for $BaCoO_{3-\delta}$ in the fixed-bed reactor.

Our group has carried out a series of basic research on perovskite materials: oxygen production performance, A/B site doping, crystal structure, oxygen non-stoichiometry, morphological properties; as well as the O_2 production performance [10, 11, 24-27]. However, there are not many documents that use cerium doped

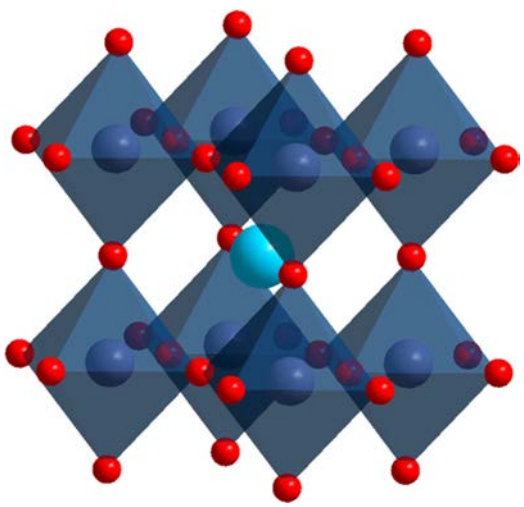

Fig. 3. The structure of perovskite ABO_3.

perovskite as an oxygen carrier. Because the oxygen carrier is the main component of the cost of the oxyfuel combustion system, the development of oxygen carrier with extraordinary oxygen desorption property and cyclic stability is the key to its actual production. In summary, Ba-based perovskite $BaCo_{0.8}M_{0.2}O_{3-\delta}$ (M = Ce, Al, Fe, Cu) doped with B-position cobalt base was selected as the research object in this paper. The purpose of this paper is to develop Ba-Co-based perovskite powders with good oxygen-enriched flow production performance as potential oxygen carrier. Furthermore, $BaCo_{0.8}Ce_{0.2}O_{3-\delta}$ (BCC) perovskite is selected as the candidate for stability tests. The optimal operation parameters of oxygen production property of BCC were studied in details.

Experimental

Sample synthesis

The EDAT sol-gel method is used for the synthesis of metal oxide powders [25]. The oxygen carriers in this study were prepared using nitrate forms such as $Ba(NO_3)_2$, $Ce(NO_3)_3$•$6H_2O$, $Co(NO_3)_2$•$6H_2O$, $Al(NO_3)_3$•$9H_2O$, $Cu(NO_3)_2$•$3H_2O$ and $Fe(NO_3)_3$•$9H_2O$. All the raw materials used are of analytic purity. Fig. 4 shows the flow diagram of the EDTA sol-gel method. The total quantity of metal ions, citric acid and EDTA were dissolved in deionized water at the molar ratio of 1:1.5:1. Subsequently, the obtained precursor solution was heated to 70 °C in a water bath and stirred until gel appeared. After the gel was formed, the gel was dried at 110 °C for 24 h. Finally, the precursor powders were sintered at 850 °C for 7 h. After sintering, the material was ground into fine powders.

Evaluation of oxygen desorption performance

The oxygen adsorption/desorption experiments of synthesized oxygen carriers are all carried out in a fixed-bed reactor under atmospheric pressure. Perovskite sample (1 g) was putted in the quartz tube. Fig. 5 shows the systematic diagram of the fixed bed system. In detail, O_2 concentration of outlet gas was measured by the online gas analyzer. Air and CO_2 were applied as the inlet gas for adsorption process and purge gas for desorption process, respectively.

For the adsorption process, the fresh perovskite powder was kept at a required temperature in air flow in 1 atm for 30 min. For the desorption process, the inlet gas was switched from air to CO_2 at a predetermined flow rate at preset desorption temperature. According to the data of the outlet gas from the online gas analyzer, the oxygen capacity was calculated using the following equation [21]:

$$m_{O_2} = \frac{\sum P \times Q \times 10^{-2} \times M_{O_2}}{V_m \times 60} \quad (2)$$

Symbol	Unit	Paraphrase
P	-	percentage of oxygen in gas products
Q	$ml \cdot min^{-1}$	gas volume flow
M_{O_2}	-	relative molecular mass of oxygen
V_m	$L \cdot mol^{-1}$	gas molar volume

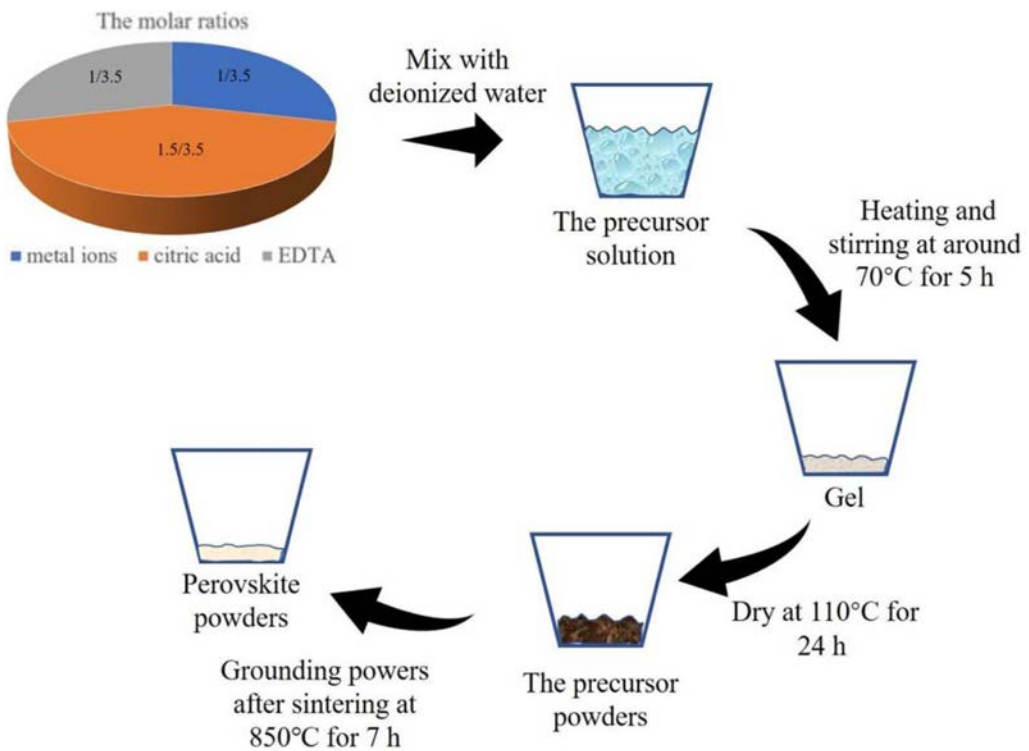

Fig. 4. Flow diagram of EDTA sol-gel method.

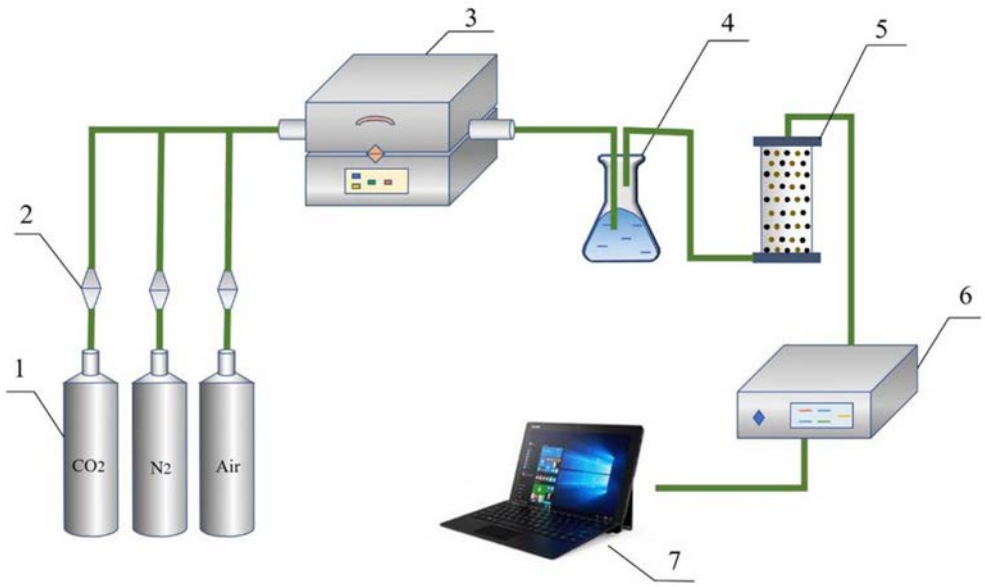

Fig. 5. Systematic diagram: (1) gas cylinder; (2) mass flow controller; (3) tube furnace; (4) condensate; (5) adsorbent; (6) online gas analyzer; (7) computerized data-acquisition system.

Results and Discussion

Impacts of the B-site doping on $BaCo_{0.8}M_{0.2}O_{3-\delta}$

Fig. 6 compares the O_2 production amount of different B-site substituted $BaCoO_{3-\delta}$ perovskites and the performance was as follows: $BaCo_{0.8}Ce_{0.2}O_{3-\delta}$ > $BaCo_{0.8}Al_{0.2}O_{3-\delta}$ > $BaCo_{0.8}Fe_{0.2}O_{3-\delta}$ > $BaCo_{0.8}Cu_{0.2}O_{3-\delta}$ at the flow rate of 200 mL·min^{-1} at 850 °C. As shown in Fig. 6, $BaCo_{0.8}Ce_{0.2}O_{3-\delta}$ demonstrate the excellent oxygen desorption performance. The oxygen production of $BaCo_{0.8}Ce_{0.2}O_{3-\delta}$ is 101.07 mg and that of $BaCo_{0.8}Al_{0.2}O_{3-\delta}$ is 99.98 mg, which are very close. $BaCo_{0.8}Ce_{0.2}O_{3-\delta}$ showed a litter more oxygen absorption amount. Therefore, $BaCo_{0.8}Ce_{0.2}O_{3-\delta}$ is selected as the candidate for the following study.

Impacts of the adsorption temperature

The adsorption temperature has impact on the oxygen adsorption capacity of the oxygen carrier, and then affects the amount of oxygen production. Fig. 7 depicts the O_2 desorption curves of $BaCo_{0.8}Ce_{0.2}O_{3-\delta}$ under various adsorption temperatures from 700 °C to 900 °C when the desorption temperature is 850 °C and the CO_2 volume flow rate is 200 mL·min^{-1}. Results indicated that the O_2 production generally increase with an increase of adsorption temperature from 700 °C to 850 °C. However, when the temperature increases to 900 °C, the value of O_2 production amount is declined to 83.58 mg. As shown in Fig. 8, $BaCo_{0.8}Ce_{0.2}O_{3-\delta}$ had maximum oxygen production at 850 °C. It is concluded that 850 °C was the optimal adsorption temperature at this condition.

Impacts of the desorption temperature

Fig. 9 and Fig. 10 compare the O_2 release capacity of

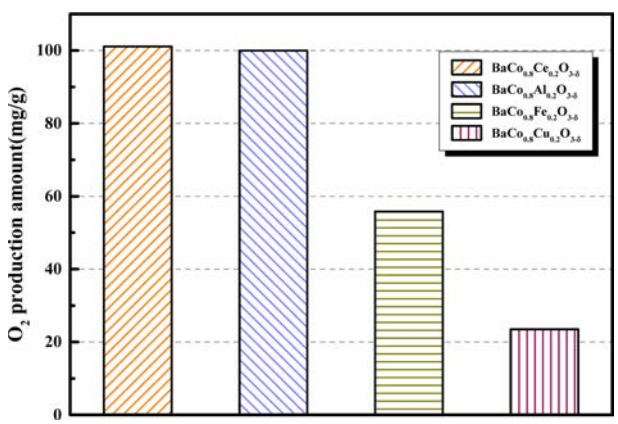

Fig. 6. O_2 production amount of different B-site doping for $BaCo_{0.8}B_{0.2}O_{3-\delta}$ (B = Ce, Al, Fe, Cu).

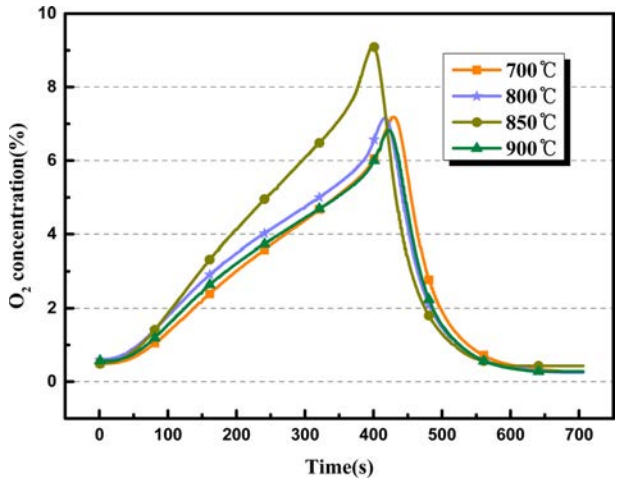

Fig. 7. Comparison of O_2 desorption curves of $BaCo_{0.8}Ce_{0.2}O_{3-\delta}$ at different adsorption temperature.

$BaCo_{0.8}Ce_{0.2}O_{3-\delta}$ at different desorption temperature (the adsorption temperature = 850 °C; the volume flow rate of CO_2 = 200 mL·min^{-1}). From Fig. 9, it can be observed that there are obvious differences in the desorption process at different desorption temperatures. When the desorption temperature is 850 °C, the slope of the curve is the maximum which indicates that the reaction rate between CO_2 and the perovskite is the highest. The oxygen quality produced by $BaCo_{0.8}Ce_{0.2}O_{3-\delta}$ is the maximum when the desorption temperature is 850 °C. $BaCo_{0.8}Ce_{0.2}O_{3-\delta}$ showed a maximum oxygen production amount of 101.07 mg at 850 °C followed by 29.78 mg, 58.22 mg, 74.97 mg, 84.3 mg and 79.89 mg, respectively. The oxygen production at 850 °C is nearly double that of 700 °C. The low temperature effect is not good because low temperature can't provide enough activation energy, and too high temperature will cause sintering, which will result in the degradation of oxygen carrier performance [11].

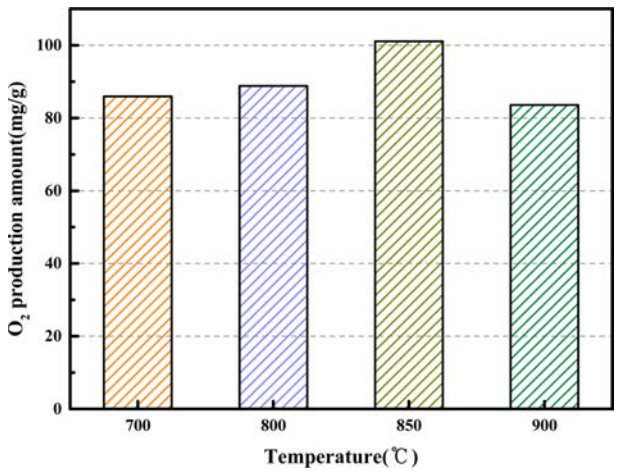

Fig. 8. Comparison of O_2 production amount for $BaCo_{0.8}Ce_{0.2}O_{3-\delta}$ at different adsorption temperatures.

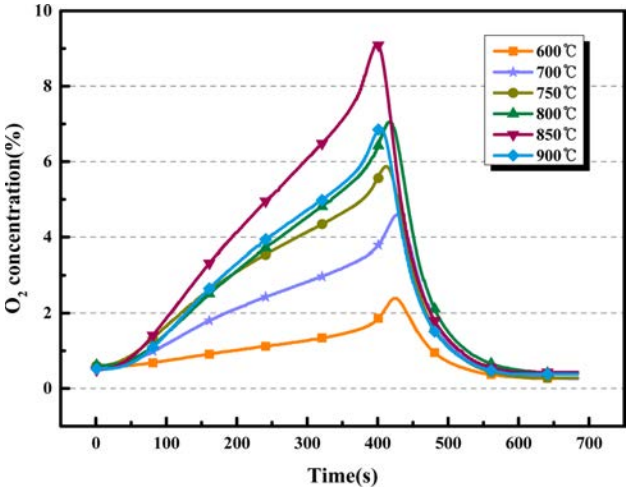

Fig. 9. Comparison of O_2 desorption curves of $BaCo_{0.8}Ce_{0.2}O_{3-\delta}$ at different desorption temperatures.

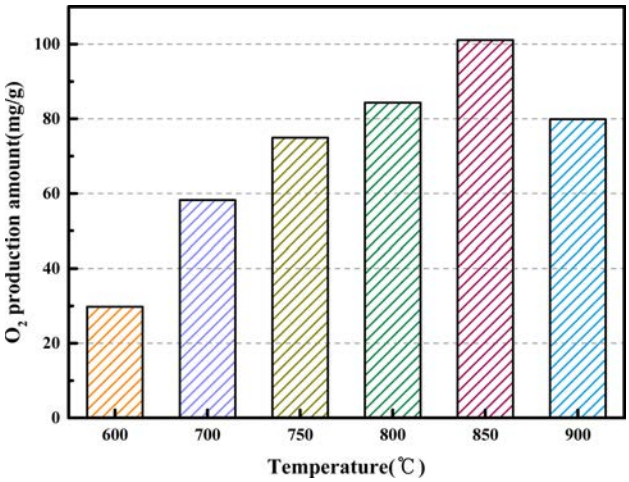

Fig. 10. Comparison of O_2 production amount for $BaCo_{0.8}Ce_{0.2}O_{3-\delta}$ at different desorption temperatures.

Effect of CO_2 volume flow rate

Fig. 11 displays the oxygen desorption property of $BaCo_{0.8}Ce_{0.2}O_{3-\delta}$ under the CO_2 volume flow rates range from 50 mL·min^{-1} to 300 mL·min^{-1} when the adsorption/desorption temperature are both 850 °C. The experimental results show that the volume flow rate of CO_2 has a considerable influence on the reaction rate of the desorption process. As the carbon dioxide purge rate increases, the response speed of the oxygen desorption process also increases significantly. Fig. 11 shows that the O_2 production of $BaCo_{0.8}Ce_{0.2}O_{3-\delta}$ is the highest when the volume flow rate is 50 mL·min^{-1}, but the desorption process is as long as 42 minutes. This is not a good choice for the industrial applications. The oxygen releasing amount of $BaCo_{0.8}Ce_{0.2}O_{3-\delta}$ is the minimum when the CO_2 volume flow rate is 300 mL·min^{-1}. This result is clear that the comprehensive performance of oxygen desorption is the best when the purge rate is 200 mL·min^{-1}.

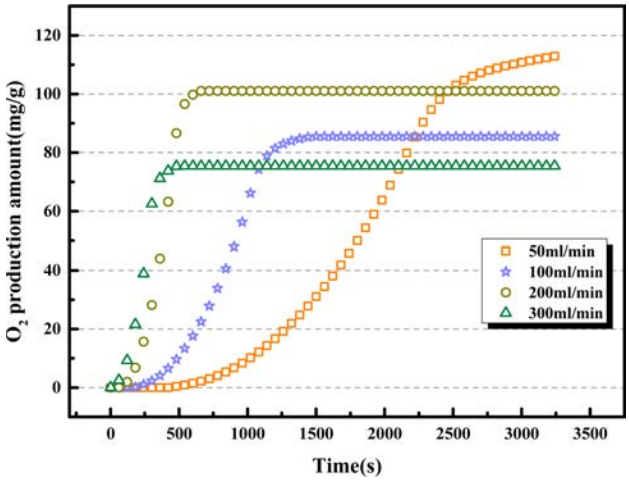

Fig. 11. Comparison of O_2 production amount of $BaCo_{0.8}Ce_{0.2}O_{3-\delta}$ at different CO_2 volume flow rates.

Impacts of the CO_2 partial pressures

The partial pressures of carbon dioxide will affect the performance of the oxygen carrier. The influence of the CO_2 partial pressures on the desorption performance of $BaCo_{0.8}Ce_{0.2}O_{3-\delta}$ were studied in details (adsorption temperature = 850 °C; desorption temperature = 850 °C; the volume flow rate of CO_2 = 200 mL·min^{-1}). The results of the oxygen production property of $BaCo_{0.8}Ce_{0.2}O_{3-\delta}$ at different CO_2 partial pressures can be seen in Fig. 12 and Fig. 13. Results indicate that the O_2 production amount decreases as the CO_2 partial pressures become higher and the oxygen concentration can be maintained at a higher level for a longer time during the entire desorption process. Therefore, the higher the partial pressure of carbon dioxide, the better the quality of the O_2-enriched stream produced.

Cyclic characteristics of the oxygen carrier

Due to the reuse of oxygen carrier in actual production activities, the cycle adsorption/desorption performance of the oxygen carrier is especially important in practical applications. Through the above experiments, the optimal adsorption/desorption temperature, partial pressure of CO_2, and CO_2 purge rate of the $BaCo_{0.8}Ce_{0.2}O_{3-\delta}$ oxygen carrier were determined for the fixed bed experiments. The stability experiment of the adsorption/desorption behavior of the oxygen carrier was carried out. From Fig. 14 and Fig. 15 show that the oxygen desorption process for each cycle is essentially the same. As shown in Fig. 14, the O_2 production decreases slightly with the increase of the number of cycles. The oxygen adsorption and desorption capacity of the oxygen carrier in the first five cycles hardly decreased, and decreased by approximately 10% after 8 cycles. The reason is that the oxygen carrier is sintered after multiple cycles, and the impurities on the surface increase, which reduces the specific surface area of the oxygen carrier and the number of oxygen vacancies. $BaCo_{0.8}Ce_{0.2}O_{3-\delta}$ oxygen carrier exhibits the good cyclic reactivity and stability and it can supply stable O_2/CO_2 cyclic gas for oxyfuel combustion.

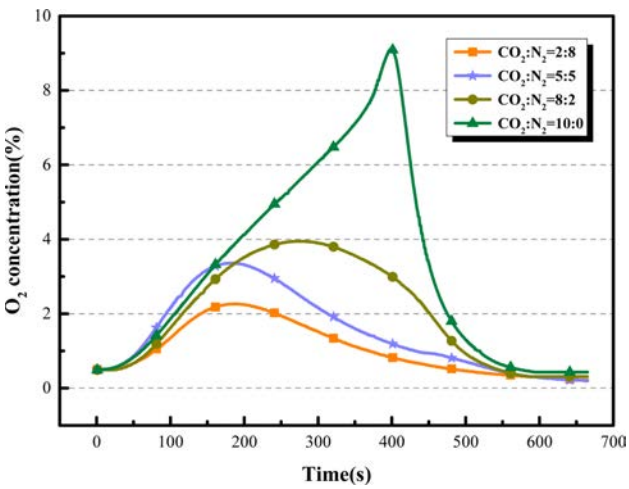

Fig. 12. Comparison of O_2 desorption curves of $BaCo_{0.8}Ce_{0.2}O_{3-\delta}$ at different CO_2 partial pressures.

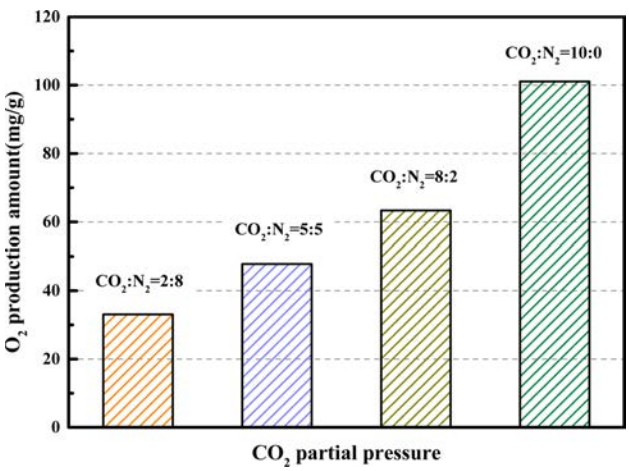

Fig. 13. Comparison of O_2 production amount for $BaCo_{0.8}Ce_{0.2}O_{3-\delta}$ at different CO_2 partial pressures.

Characteristics of perovskites

The micromorphology and microstructure of the

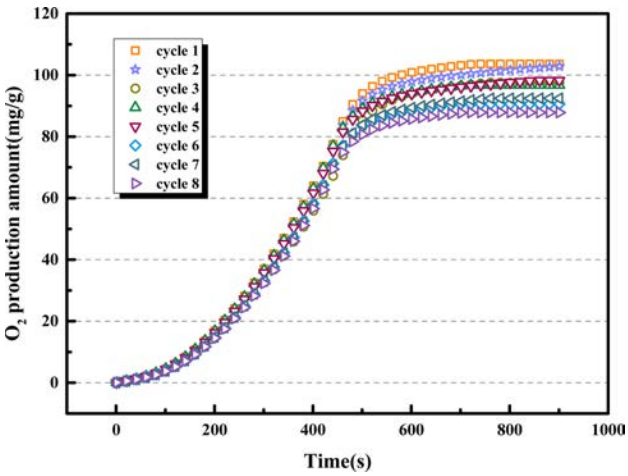

Fig. 14. Comparison of cyclic O_2 production amount of $BaCo_{0.8}Ce_{0.2}O_{3-\delta}$.

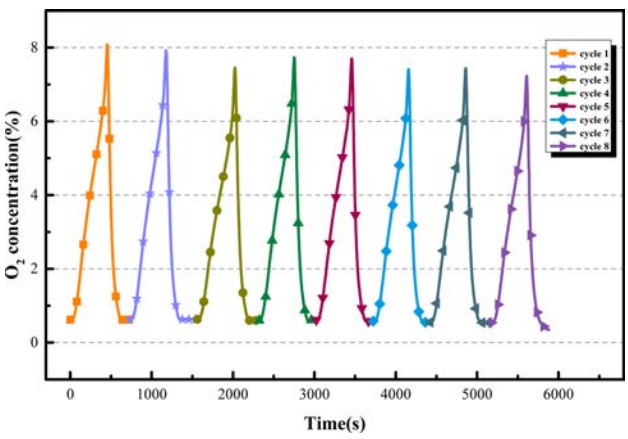

Fig. 15. Cyclic capability of $BaCo_{0.8}Ce_{0.2}O_{3-\delta}$.

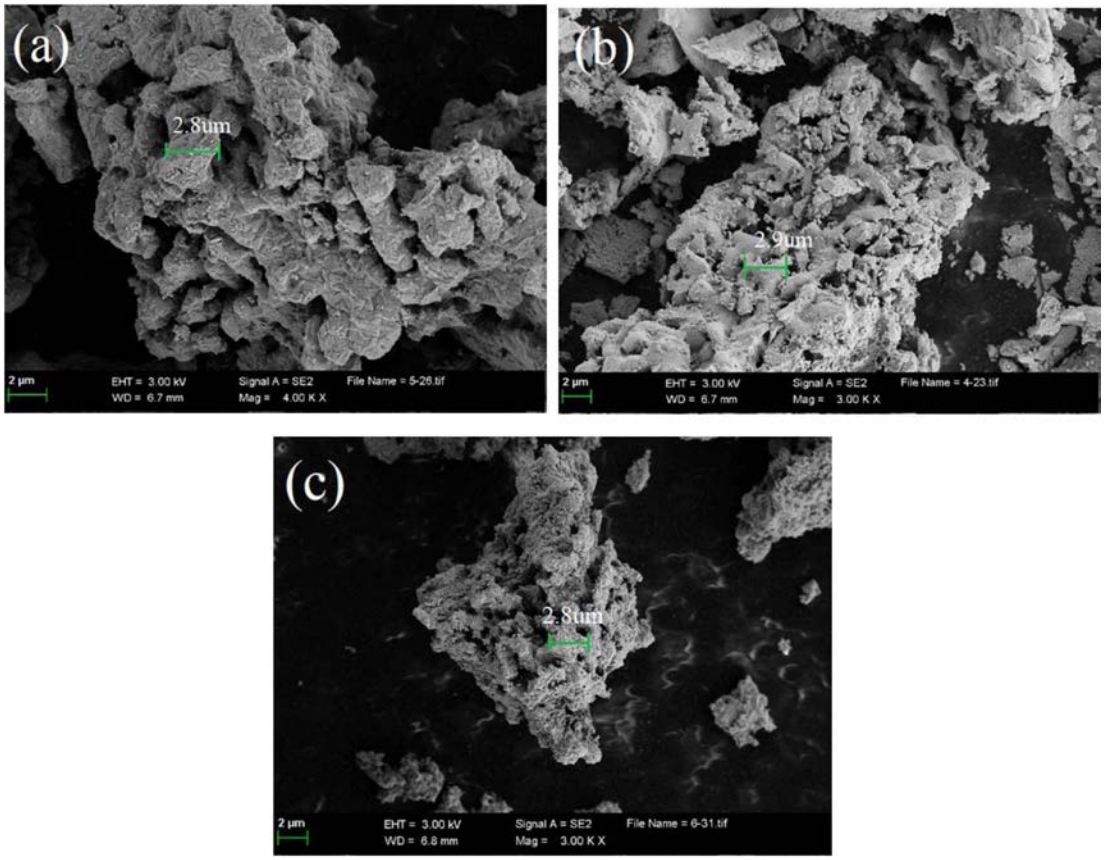

Fig. 16. SEM images of $BaCo_{0.8}Ce_{0.2}O_{3-\delta}$: (a) fresh sample (4000×), (b) spent sample (3000×), (c) regenerative sample after 8 cycles (3000×).

$BaCo_{0.8}Ce_{0.2}O_{3-\delta}$ perovskite powders were examined by SEM characteristics. As shown in Fig. 16(a), at magnification of 4000, the fresh sample presents a porous structure, and it can be observed that a lot of pores around 1-2 um in size are distributed inside the sample particles. Fig. 16(b) shows the sample after desorption and the particle size distribution is in the range of 0.5-1.5 um. The pores on the surface of the particles become smaller or disappear, and the particles become fuller, and the surface is covered with impurities. The fixed bed cycle test shows that the oxygen production amount decreased by approximately 10% after 8 cycles, indicating that the disappearance of micropores and the coverage of impurities lead to a decrease in oxygen release performance. Fig. 16(c) shows the sample after the fixed bed cyclic test. Compared with Fig. 16(a), the small pores inside the particles are reduced, and the covered impurities are further increased. The specific surface area and porosity of samples are important factors affecting gas-solid reaction. This corroborates the result shown in Fig. 14.

Conclusions

In the present study, the Ba-Co-based perovskite powders was synthesized and applied for producing O_2-enriched CO_2 gas. The fixed-bed experiments showed that the performance of synthesized perovskites for as follows: $BaCo_{0.8}Ce_{0.2}O_{3-\delta}$ > $BaCo_{0.8}Al_{0.2}O_{3-\delta}$ > $BaCo_{0.8}Fe_{0.2}O_{3-\delta}$ > $BaCo_{0.8}Cu_{0.2}O_{3-\delta}$. The oxygen production yield of $BaCo_{0.8}Ce_{0.2}O_{3-\delta}$ perovskite powders is as high as 101.07 mg/g. The optimum temperature for both adsorption and desorption processes was determined to be 850 °C. In addition, the experimental results show that the optimal volume flow rate of CO_2, and CO_2 partial pressures on $BaCo_{0.8}Ce_{0.2}O_{3-\delta}$ perovskite powders were determined to be 200 $ml \cdot min^{-1}$, 100% CO_2 partial pressure, respectively. The results of multiple cyclic tests showed that $BaCo_{0.8}Ce_{0.2}O_{3-\delta}$ perovskite possess high performance and cycle stability. SEM results showed that the fresh samples of $BaCo_{0.8}Ce_{0.2}O_{3-\delta}$ had a porous structure, and the particles were covered by impurities after the cycle due to sintering. This work showed that $BaCo_{0.8}Ce_{0.2}O_{3-\delta}$ and its derivatives are promising materials for producing O_2-enriched CO_2 mixed gas for oxyfuel combustion technique.

Acknowledgments

This work was supported by the Natural Science Foundation of Liaoning Province (No.2019-ZD-0154 and No. 2020-HYLH-38), the Fundamental Research Funds for the Central Universities of China (No. 3132019327) and Dalian City Innovative Support

Program for High-Level Talents (No. 2019RQ036).

References

1. C.G. Zheng, Z.H. Liu, J. Xiang, L.Q. Zhang, S.H. Zhang, C. Luo, and Y.C. Zhao, Engineering 1[1] (2015) 139-149.
2. T. Bruckner, Energy Technol. 4[1] (2016) 19-30.
3. H.N. Jang, J.H. Kim, S.K. Back, J.H. Sung, H.M. Yoo, H.S. Choi, and Y.C. Seo, Fuel 170 (2016) 92-99.
4. F. Carrasco-Maldonado, R. Spörl, K. Fleiger, V. Hoenig, J. Maier, and G. Scheffknecht, Int. J. Greenh. Gas Control 45 (2016) 189-199.
5. H.B. Wu, Y. Zhang, W. Chen, Z.H. Liu, T. Zhang, Q. Sun, and Z.M. Zheng, Fuel 263 (2020) 116799.
6. Y.H. Jiang, Q.W. Shen, S.A. Li, G.G. Yang, and N.B. Huang, New J. Chem. 44[15] (2020) 6003-6009.
7. Q. Yang, Y.S. Lin, and M. Bülow, AIChE J. 52[2] (2006) 574-581.
8. B.J.P. Buhre, L.K. Elliott, C.D. Sheng, R.P. Gupta, and T.F. Wall, Prog. Energy Combust. Sci. 31[4] (2005) 283-307.
9. Q.H. Yin, J. Kniep, and Y.S. Lin, Chem. Eng. Sci. 63[8] (2008) 2211-2218.
10. Q.W. Shen, Y.D. Zhang, H.R. Ding, L.J. Wu, Y.Q. Xu, B.C. Shi, Y. Zheng, and J.L. Yuan, Energies 10[2] (2017) 164-174.
11. Q.W. Shen, Y. Zheng, C. Luo, N. Ding, C.G. Zheng, and M. Thern, RSC Adv. 5 (2015) 39785-39790.
12. Q.W. Shen, Y.H. Jiang, S.A. Li, X.R. Lv, G.G. Yang, and B. Sunden, Int. J. Energy Res. 44[8] (2020) 6991-6999.
13. Q.W. Shen, Y.H. Jiang, F.H. Xia, B. Wang, X.R. Lv, W.Q. Ye, and G.G. Yang, Pet. Sci. Technol. 38[6] (2020) 618-625.
14. H.Z. Song, J.F. Jia, S.M. Zhang, D.L. Yang, H.W. Sun, and X. Hu, Mater. Res. Bull. 47[3] (2012) 518-520.
15. J.P. Correa-Baena, A. Abate, M. Saliba, W. Tress, T. Jesper Jacobsson, M. Grätzel, and A. Hagfeldt, Energy Environ. Sci. 10 (2017) 710-727.
16. F.T.Z. Toma, I.N. Esha, M. Al-Amin, M.N.I. Khan, and K.H. Maria, J. Ceram. Process. Res. 18[10] (2017) 701-710.
17. A. El Ghandouri, S. Sayouri, T. Lamcharfi, and L. Hajji, J. Ceram. Process. Res. 19[2] (2018) 154-170.
18. Q.Y. Wang, C. Luo, X.S. Li, H.R. Ding, C. Shen, D.S. Cao, and L.Q. Zhang, J. CO2 Util. 32 (2019) 163-169.
19. D.N. Mueller, R.A. De Souza, H.I. Yoo, and M. Martin, Chem. Mater. 24[2] (2012) 269-274.
20. M. Karppinen, H. Yamauchi, S. Otani, T. Fujita, T. Motohashi, Y.H. Huang, M. Valkeapää, and H. Fjellvåg, Chem. Mater. 18[2] (2006) 490-494.
21. S.A. Li, R.Q. Wei, Y.H. Jiang, Q.W. Shen, G.G. Yang, and N.B. Huang, J. Ceram. Process. Res. 21[1] (2020) 64-68.
22. H.R. Ding, Y.Q. Xu, C. Luo, Q.Y. Wang, C. Shen, J.X. Xu, and L.Q. Zhang, Energy Convers. Manag. 171 (2018) 12-19.
23. Q.W. Shen, S.A. Li, G.G. Yang, J.L. Yuan, and N.B. Huang, J. Ceram. Process. Res. 20[2] (2019) 152-157.
24. H.R Ding, Y.Q. Xu, C. Luo, Q.Y. Wang, S. Li, G.Q. Cai, L.Q. Zhang, Y. Zheng, and Q.W. Shen, Chem. Eng. J. 323 (2017) 340-346.
25. Q.W. Shen, Y. Zheng, S.A. Li, H.R. Ding, Y.Q. Xu, C.G. Zheng, and M. Thern, J. Alloys Compd. 658 (2016) 125-131.
26. Q.W. Shen, S.A. Li, G.G. Yang, B. Sunden, and J.L. Yuan, Energies 12[3] (2019) 410-420.
27. Q.W. Shen, Y. Zheng, C. Luo, and C.G. Zheng, Bull. Korean Chem. Soc. 35[6] (2014) 1613-1618.